Electric Power Systems Research 187 (2020) 106451

Contents lists available at ScienceDirect

Electric Power Systems Research

journal homepage: www.elsevier.com/locate/epsr

DC-bus Voltage Control based on Direct Lyapunov Method for a Converter-based Stand-alone DC Micro-grid

Arash Abedi, Behrooz Rezaie*, Alireza Khosravi, Majid Shahabi

Department of Electrical and Computer Engineering, Babol Noshirvani University of Technology, Babol, IRAN

ARTICLE INFO

Keywords:
DC micro-grid
voltage control
direct Lyapunov method
stability analysis
switching function
DC/DC converter

ABSTRACT

This paper presents a novel distributed control technique based on the direct Lyapunov method to regulate the DC-bus voltage of a stand-alone DC micro-grid with variant power generation and consumption. This DC micro-grid consists of a photovoltaic unit, a wind-turbine unit, a micro-turbine unit, and a lithium-battery-based energy storage unit, where the energy storage system is constantly connected to the DC-bus in order to damp any DC voltage alteration. Moreover, the micro-turbine unit is set to compensate for the lack of power when a significant decrement in the generated power or a severe increment in the load power happens. In these types of energy multi-sources systems with the voltage instability, a proper distributed control technique focusing on the voltage stabilization through the current regulation of DC/DC converters is required to decrease the associated fluctuation impact of power-sharing. This paper proposes a control technique based on the comprehensive differential models of the power-converter-based generation units in which both the steady-state and dynamic operating conditions of the DC/DC converters are considered. Moreover, the stability of the generation units is analyzed using an input-output linearization technique. Simulation results in MATLAB/SIMULINK environment verify the accuracy of the energy-management-based control strategy in various operating conditions.

1. Introduction

The use of renewable energy resources (RERs) such as photovoltaic (PV) and wind-turbine units has been intensely growing in recent years as a substantial aim to reduce dependency on fossil fuels, and thereby to decrease greenhouse gas emissions and prevent global warming [1]. The RERs can be used in various forms such as DC micro-grid [2], AC micro-grid [[3], [4]] and the distributed generation (DG) resources integrated into power grid [5].

Micro-grid is a small model of an active distribution network employing DGs (both renewable and conventional), energy storage systems and loads, which operates either in grid-connected or islanded mode. Variety of energy resources in the micro-grid increases the efficiency, reliability, power quality and reduces the power losses. Moreover, for isolated or remote areas where supplying electricity through transmission lines is impossible, the stand-alone micro-grid is an attractive alternative.

In a stand-alone micro-grid supplying the consumption loads of the buildings, most of the electric devices such as computers, mobile phones, and multimedia work using DC power supply. There are also other loads in this kind of micro-grids such as the lighting and the air-conditioning equipment that can be supplied either with DC or AC power sources. Supplying and distributing energy in DC form is beneficial as it provides advantages such as the reduced number of converters, limited control challenges in the DC system comparing to the AC system with frequency variations and the minimized cost. Therefore, the stand-alone DC micro-grid is an appropriate choice for supplying remote areas [6–8]. This enforced researchers to pay more attention to the methods of voltage regulation and energy management [[9], [10]].

Many studies have focused on the DC-bus voltage stability and energy-management-based controllers from different points of views [6,7]. A model predictive control technique for an AC-DC-AC converter has been designed in [11] to use the maximum power of the wind-turbine system embedded in a micro-grid including a direct drive wind generator and a battery storage system. In addition, for stable operation in both grid-connected and islanding modes, a supervisory method has been proposed in order to coordinate the performance of the wind system and the battery unit, regardless of the dynamics of the converters and their vital role in voltage fluctuations. In [12], an independent 3-level control technique has been employed to a DC micro-grid in which various operating conditions such as load variations, the generation changes like as the islanding-mode, grid reconnection, and a load shedding have been considered with the aim of stabilizing the DC-

* Corresponding author.
E-mail address: brezaie@nit.ac.ir (B. Rezaie).

https://doi.org/10.1016/j.epsr.2020.106451
Received 20 September 2018; Received in revised form 31 May 2020; Accepted 31 May 2020
Available online 15 June 2020

bus voltage. Xu *et al.* in [13] have designed a DC voltage control system in which the wind-turbine system is accurately coordinated with an embedded energy storage system. In all the aforementioned references, the ideal converters have been used, and the control challenges related to the dynamics of the converters and the control of switching functions or duty-cycle have not been investigated.

Furthermore, different control strategies have been proposed to control the converters associated with the RERs and the DC-voltage-regulation-based energy management, focusing more on the switching functions and the duty-cycle of the converters [[14], [15]]. In these studies, non-ideal models for converters have been used. Considering the dynamic effects of these non-ideal converters makes the results of the study more realistic. In [8], a frequency-based method has been considered for decreasing the DC-bus voltage fluctuations and the energy management has been presented in a DC micro-grid consisting of a wind turbine, PV panels, a diesel generator, and the energy storage device. In the presence of battery and super-capacitor-based energy storage systems, a polynomial control strategy has been designed in [16] for controlling DC/DC converters in order to regulate the DC-bus voltage and perform the current management. In this work, the simplified non-ideal converter models have been used. In these studies, supercapacitor quickly compensates high power fluctuations. However, the steady-state oscillations caused by the converter dynamics have not been investigated in the control scheme. Three DC/DC converters for PV arrays, two DC/AC converters, and one DC/DC converter for battery operation and local loads have been constructed in [17] as a modular PV generation system. In this strategy, an improved DC-bus signaling-based distributed control technique has been proposed to enhance the reliability and efficiency of the considered generation system. A coordinated control technique for a DC micro-grid included the battery system, wind-turbine, and load-shedding-based management has been analyzed in [18]. Control strategies for DC micro-grid-based converters in both grid-connected and islanding modes as well as the battery-integrated DC/DC converters have been accurately investigated in references [19–21]. Rashad *et al.* in [22], have accomplished a stability analysis of a DC micro-grid based on mathematical modeling and based on this analysis they have also employed sliding mode hysteresis controller. Moreover, a new control technique based on two revolving field theories (TRFT) has been proposed in [23] to control a DC micro-grid in the presence of a single-phase static and dynamic AC loads. In additions, several studies in [24–27] have dealt with several new droop-based control techniques for regulating the operation of the considered micro-grid. In [27], a droop control technique completed with the virtual voltage axis has been designed for a DC microgrid to provide coordination between the voltage restoration and the energy management. In fact, the virtual voltage axis can help the DC micro-grids to have less voltage deviation and good energy management performance with the operation band. A converter-based control of DC micro-grid including the battery-supercapacitor based on hybrid energy storage system has been designed and analyzed in [28]. In this study, the sensitivity of DC micro-grid stability in the presence of the supercapacitor voltage variation and an optimal supercapacitor voltage has been investigated. In [29], stability analysis and stabilization of DC micro-grid with multiple parallel-connected DC/DC converters have been provided. In this method, by identifying the eigenvalues of the Jacobian matrix, the stability domains have been determined through the constraints of capacities, inductances, maximum load power, and distances of the cables regarding DC micro-grid. A nonlinear stability analysis has also been performed in [30] for a DC micro-grid by the use of decreasing the numbers of differential equations to accomplish the prediction of the micro-grid behavior. Although the advantages of the existing studies are significant, in the mentioned researches, the dynamic part of the converter switching functions has not been considered separately to design controllers. Considering these dynamic parts in designing controllers of switching functions can cause satisfactory results in all conditions and an appropriate stable response in the steady-state with a quick transient-state response under variations of load and power can be reached. This motivates us in the proposed controller to separate the dynamic effects of the independent state variables errors of the converter from the switching function and consequently, to reduce the current and voltage fluctuations.

- In this paper, a control strategy with an effective stability analysis based on direct Lyapunov method (DLM) is proposed to perform the DC-bus voltage regulation of a stand-alone DC micro-grid consisting of the wind-turbine unit, PV units, gas micro-turbine unit, and the lithium-battery-based energy storage system. In this work, compared with the existing studies, a more effective stability analysis without reducing the order of the converters dynamical models based on the Lyapunov theory is presented which can provide asymptotic stability of the system. The objective is to stabilize the DC-bus voltage through the accurate and fast regulation of the output currents of the converters with minimum dynamic fluctuations. In the proposed method, control of switching functions for the buck and bidirectional buck-boost DC/DC converters with relying on the dynamic components is achieved through the DLM. Moreover, the stability of the generation units is investigated using an input-output linearization (IOL) technique. Therefore, the main contributions of this paper are:
- Proposing a novel control technique for the DC/DC converters connected to a stand-alone DC micro-grid by separating the dynamic and steady-state components regarding switching functions.
- Presenting an accurate regulation algorithm for the output currents of the generation units based on the energy analysis of DLM to guarantee and enhance the DC-link voltage stability with considering the errors of the electrical state variables.
- Stability analysis of the generation units is performd using IOL method and appropriate control law is obtained.

The most prominent features of this design are the simplicity, the easy execution, the fast performance, negligible steady-state fluctuations with very swift transient-state response, distributed control ability with minimum need for communications between the controllers, functionality in the multi-source and the mono-source generation mode, and the developable structure of micro-grids with the ability of plug-and-play without the need to restructure the controllers.

The paper is organized as follows. Firstly, in Section 2, a comprehensive dynamic model of the proposed system is presented. Then, the steady-state mode of all units is considered. In Section 3, the proposed method is described. In this section, after the steady-state analysis, IOL technique is utilized to analyze the stability of the generation units, and then DLM is applied to four DC/DC converter-based models and accurate controllers are designed. Moreover, a dynamic assessment of the proposed controllers is accurately investigated. The simulation results are presented in Section 4, and the conclusion is drawn in the last section.

2. Multi Sources DC Micro-grid

The general structure of the considered DC micro-grid is illustrated in Fig. 1. It can be observed that this structure consists of a photovoltaic unit (PVU), a wind-turbine generation unit (WGU), a micro-turbine generation unit (MGU) and an energy storage system. A lithium-battery unit (LBU) is employed as the energy storage system to provide a constant DC-bus voltage for loads connected to the DC micro-grid in the steady-state operation or under dynamic changes due to the load alterations. The power generation systems should compensate for the DC-bus voltage variations caused by the load fluctuations in the DC micro-grid. In this section, the detailed dynamical models of these power generation systems are described.

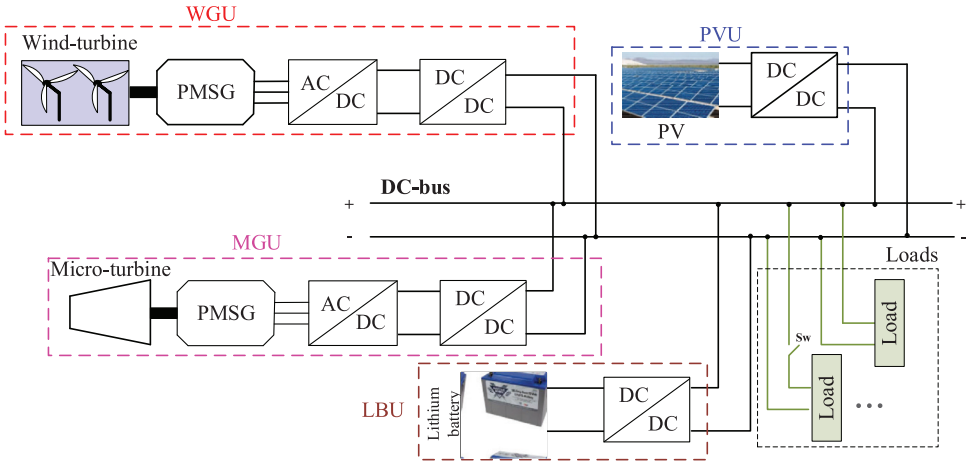

Fig. 1. Proposed DC Micro-grid configuration.

2.1. PVU Dynamic Model

An overall description of a PVU used in the DC micro-grid is depicted in Fig. 2. This unit consists of two parts including the photovoltaic cells and the buck DC/DC converter. For the first part of the PVU, as shown in Fig. 2.a, the light-generated current is in parallel connection with a diode D_p and a shunt resistanceR_1, while the connections between the cells are modeled by small series resistance R_2. The relationship between the output current and voltage of the photovoltaic cell is formulated as equation (1) [8]:

$$i_{i1} = n_p i_{ph} - n_p I_{rs}\left[e^{(q(v_{n1}+i_{n1}R_2)/(n_s AT))} - 1\right] \quad (1)$$

where v_{n1}, $i_{n1}$and i_{i1} are respectively the output voltage, the output current of each cell and the output current of the PV panel with n_s cells in series and n_p cells in parallel. Moreover, q is the electron charge, A is the ideality factor and T is the temperature in Kelvin. In addition, I_{rs} and i_{ph} are the cell reverse saturation current and the light-generated current respectively and can be approximated as [8]:

$$I_{rs} \approx K_0(T)^3 e^{(-E_{go}/KT)} \quad (2)$$

$$i_{ph} \approx (I_{sc} + K_I(T - T_r))\lambda/100 \quad (3)$$

where E_{go} is the gap energy of the semiconductor, K and K_0 are the Boltzmann constant and the temperature coefficient in reverse current equation, respectively. Moreover, I_{sc} is the short circuit current, λ the irradiation of sun, K_I represents the temperature coefficient corresponding to short circuit current, and T_r expresses the reference of temperature in Kelvin. From (1), the input voltage of the buck DC/DC converter can be obtained as:

$$v_{i1} = n_s v_{n1} \quad (4)$$

wherev_{i1}, is the output voltage of the PV panel.

Since the injected power from PVU to the DC micro-grid is accomplished by a buck DC/DC converter, a complete dynamic description of this converter is required. Considering the second part of Fig. 2.b, the dynamical features of the buck DC/DC converter can be modeled as:

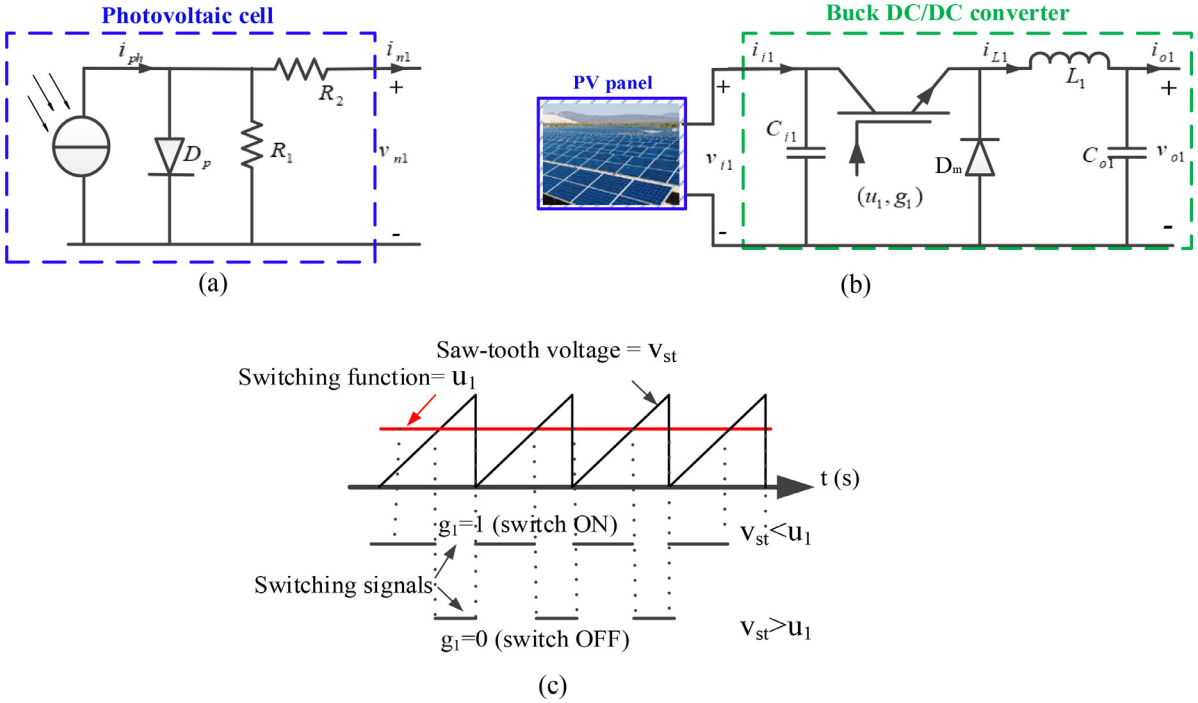

Fig. 2. The detailed structure of (a) photovoltaic cell, (b) PVU (c) switching signal generating by PWM.

$$\frac{dv_{i1}}{dt} = \frac{i_{i1}}{C_{i1}} - \frac{i_{L1}u_1}{C_{i1}} \tag{5}$$

$$\frac{di_{L1}}{dt} = \frac{v_{i1}u_1}{L_1} - \frac{v_{o1}}{L_1} \tag{6}$$

$$\frac{dv_{o1}}{dt} = \frac{i_{L1}}{C_{o1}} - \frac{i_{o1}}{C_{o1}} \tag{7}$$

where C_{i1}, C_{o1}, L_1, u_1, and i_{L1} are the input capacitor, the output capacitor, the inductance, and the switching function of the converter, and inductance current respectively. In order to provide an accurate operation for the PV-based converter, the control of the output voltage v_{o1} and the output current i_{o1} in (5)-(7) should be executed based on the operating point of other power generation units in the proposed DC micro-grid system that is discussed in the related section. Fig. 2.c shows the relation between the switching function (u_1) and the switching signals (g_1). The switching signal is generated as the output of a control process by applying the switching function to the pulse width modulation (PWM).

2.2. WGU Dynamic Model

The wind-turbine system along with permanent magnet synchronous generator (PMSG), is connected to the DC-bus of the proposed DC micro-grid, as shown in Fig. 3. The generated power of the wind-turbine can be converted to a constant DC power in two stages through the PMSG and three-phase diode rectifier respectively, as depicted in Fig. 3. Then, the required DC power for the proposed DC micro-grid is supplied by using a buck DC/DC converter. Thus, the dynamic model of the PMSG in the stand-alone DC micro-grid can be achieved as follows [31]:

$$\frac{di_{dw}}{dt} = -\frac{R_{eqw}i_{dw}}{L_{eqw}} + \omega_{ew}i_{qw} \tag{8}$$

$$\frac{di_{qw}}{dt} = -\frac{R_{eqw}i_{qw}}{L_{eqw}} - \omega_{ew}i_{dw} - \frac{\varphi_{mw}}{L_{eqw}}\omega_{ew} \tag{9}$$

$$\frac{d\omega_{ew}}{dt} = \frac{p_w}{J_w}T_{tw} - \frac{3}{2}\frac{p_w^2}{J_w}\varphi_{mw}i_{qw} \tag{10}$$

where i_{dw} and i_{qw} are the PMSG stator currents in the d-q reference frame, R_{eqw}, L_{eqw} and J_w are respectively the equivalent resistance and inductance seen from the stator terminals, and the inertia moment of the wind-turbine and PMSG. In these equations, ω_{ew}, φ_{mw}, T_{tw} and p_w represent respectively the angular frequency, the flux, the wind-turbine mechanical torque and the pole pair number of PMSG in the WGU. More information about the modeling of the mechanical parts of the WGU can be found in [32]. According to the second part of Fig. 3, the dynamic description of the buck DC/DC converter can be written as:

$$\frac{dv_{i2}}{dt} = \frac{i_{i2}}{C_{i2}} - \frac{i_{L2}u_2}{C_{i2}} \tag{11}$$

$$\frac{di_{L2}}{dt} = \frac{v_{i2}u_2}{L_2} - \frac{v_{o2}}{L_2} \tag{12}$$

$$\frac{dv_{o2}}{dt} = \frac{i_{L2}}{C_{o2}} - \frac{i_{o2}}{C_{o2}} \tag{13}$$

where C_{i2}, C_{o2}, L_2, and u_2 are respectively the input capacitor, the output capacitor, the inductance, and the switching function of the converter. In addition, i_{L2} is the inductance current, v_{o2} the output voltage of the converter and i_{o2} the output current of the converter that represents the contribution of the WGU in the DC-bus.

Based on equations (8)-(13), v_{i2} and i_{i2} are respectively the input voltage and current of the converter that are the rectified output voltage and current of the PMSG, can be affected by PMSG operation, where $i_{i2} = (\pi/2\sqrt{3})\sqrt{i_{dw}^2 + i_{qw}^2}$. Thus, the equations (8)-(13) can be used for controlling the DC power injected from the WGU into the DC-bus.

2.3. MGU Dynamic Model

Fig. 4 shows the overall structure of the considered micro-turbine-based PMSG connected to the DC-bus of the DC micro-grid by a buck DC/DC converter. As shown in Fig. 4, a three-phase diode rectifier is employed to make the connection between the PMSG and the DC/DC converter. In this structure, the buck DC/DC converter plays the main role in injecting the needed DC power into DC-bus. The dynamic model of the PMSG used in micro-turbine-based power generation unit can be obtained as [31]:

$$\frac{di_{dm}}{dt} = -\frac{R_{eqm}i_{dm}}{L_{eqm}} + \omega_{em}i_{qm} \tag{14}$$

$$\frac{di_{qm}}{dt} = -\frac{R_{eqm}i_{qm}}{L_{eqm}} - \omega_{em}i_{dm} - \frac{\varphi_{mm}}{L_{eqm}}\omega_{em} \tag{15}$$

$$\frac{d\omega_{em}}{dt} = \frac{p_m}{J_m}T_{tm} - \frac{3}{2}\frac{p_m^2}{J_m}\varphi_{mm}i_{qm} \tag{16}$$

where i_{dm}, i_{qm}, R_{eqm}, L_{eqm} and J_m are respectively the PMSG stator currents in the d-q reference frame, the equivalent resistance, and inductance seen from the stator terminals, and the inertia moment of the micro-turbine and PMSG. In the above equations, ω_{em}, φ_{mm}, T_{tm} and p_m represent respectively the angular frequency, the flux, the micro-turbine mechanical torque and the pole pair number of PMSG in the MGU. More information about the modeling of the mechanical parts of the MGU can be found in [33]. Considering the second part of Fig. 4, the dynamic model of the buck DC/DC converter employed in MGU is written as:

In the above equations, ω_{em}, φ_{mm}, $T_{tm}$and p_m represent respectively the angular frequency, the flux, the micro-turbine mechanical torque and the pole pair number of PMSG in the MGU. More information about the modeling of the mechanical parts of the MGU can be found in [33]. Considering the second part of Fig. 4, the dynamic model of the buck DC/DC converter employed in MGU is written as:

$$\frac{dv_{i3}}{dt} = \frac{i_{i3}}{C_{i3}} - \frac{i_{L3}u_3}{C_{i3}} \tag{17}$$

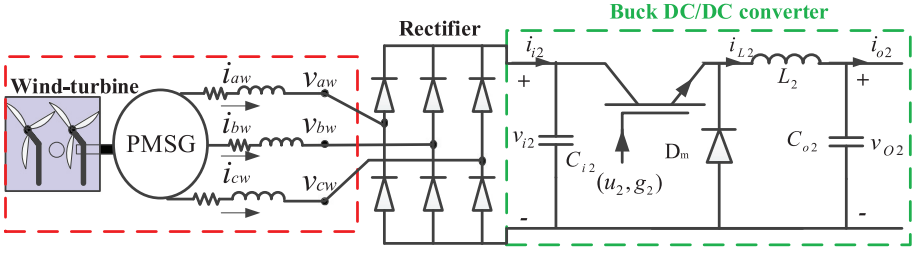

Fig. 3. The detailed structure of WGU.

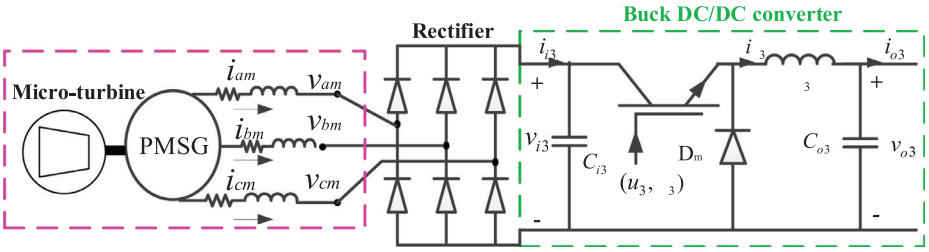

Fig. 4. The detailed structure of MGU.

$$\frac{di_{L3}}{dt} = \frac{v_{i3}u_3}{L_3} - \frac{V_{o3}}{L_3} \tag{18}$$

$$\frac{dv_{o3}}{dt} = \frac{i_{L3}}{C_{o3}} - \frac{i_{o3}}{C_{o3}} \tag{19}$$

where C_{i3}, C_{o3}, L_3, u_3 are respectively the input capacitor, the output capacitor, the inductance, the switching. Moreover, i_{L3} is the inductance current, v_{o3} is the output voltage and i_{o3} is the output current of the converter that represents the contribution of the MGU in the DC-bus. v_{i3} and i_{i3} are respectively the input voltage and current of the converter that are the rectified output voltage and current of the PMSG, can be affected by PMSG operation, where $i_{i3} = (\pi/2\sqrt{3})\sqrt{i_{dm}^2 + i_{qm}^2}$. Thus, the equations (14)-(19) can be used for controlling the DC power injected from the MGU into the DC-bus.

2.4. LBU Dynamic Model

The LBU consists of two parts. The first part is responsible to provide a DC-bus voltage for the second part. The general structure of LBU is shown in Fig. 5. Based on this scheme, the dynamic equation of the first part output voltage can be achieved as below [8]:

$$R_C C_C \frac{dv_{i4}}{dt} + v_{i4} = V_{EMF} - R_\Omega R_C C_C \frac{di_{i4}}{dt} - (R_\Omega + R_C) i_{i4} \tag{20}$$

where R_Ω is an internal series resistance. According to Fig. 5, a parallel RC circuit, consisting of R_C and C_C describes the charge transfer and the diffusion process between the electrode and the electrolyte. In addition, V_{EMF} is the open-circuit voltage of the battery, v_{i4} and i_{i4} are the input voltage and current of the second part of LBU that is a bidirectional buck-boost DC/DC converter as depicted in Fig. 5. According to this figure, the dynamic description of this converter can be written as:

$$\frac{di_{L4}}{dt} = \frac{v_{i4}}{L_4} - u_4 \frac{v_{o4}}{L_4} \tag{21}$$

$$\frac{dv_{o4}}{dt} = u_4 \frac{i_{L4}}{C_{o4}} - \frac{i_{o4}}{C_{o4}} \tag{22}$$

where C_{o4}, L_4, and u_4 are respectively the capacitor, the inductance, and the switching function of the buck-boost converter. Moreover, i_{L4} is the inductance current, v_{o4} presents the output voltage of the converter and i_{o4} is the output current of the converter that represents the contribution of the LBU in the DC-bus. The considered bidirectional buck-boost DC/DC converter should focus on controlling the output state variables of v_{o4} and i_{o4}. In fact, the dynamic equations (21)-(22) are used for the aim of regulating the DC-bus of DC micro-grid when the LBU is needed. It should be noticed that in equations (5)-(7), (11)-(12), (17)-(18), and (21)-(22), the average values of switching states u_j, for $j = 1, \ldots, 4$ are considered instead of the instantaneous switching signals (g_j).

3. The Proposed Controller Technique

In the proposed control strategy, all operating conditions are considered and the subsequences, as well as the DC power-sharing amount of each generation unit including PVU, WGU, MGU, and LBU, are accurately specified. In this section, both steady-state and the dynamic analysis of the proposed controller are investigated.

3.1. Steady-State Analysis

In order to control the DC-bus voltage of the proposed DC micro-grid in the steady-state operation, the switching functions of all DC power generators embedded in the dynamic equations of (5)-(22) should be achieved by substituting the desired values of all state variables, identified by '*' superscripts, in the related equations as:

$$\begin{cases} \frac{dv_{ij}^*}{dt} = \frac{i_{ij}^*}{C_{ij}} - \frac{i_{Lj}^* u_j^*}{C_{ij}} \\ \frac{di_{Lj}^*}{dt} = \frac{v_{ij}^* u_j^*}{L_j} - \frac{v_{oj}^*}{L_j} \end{cases} \cdot j = 1, 2, 3$$

$$\frac{di_{L4}^*}{dt} = \frac{v_{i4}^*}{L_4} - u_4^* \frac{v_{o4}^*}{L_4}$$

$$\frac{dv_{o4}^*}{dt} = u_4^* \frac{i_{L4}^*}{C_{o4}} - \frac{i_{o4}^*}{C_{o4}} \tag{23}$$

Thus, using (23), and according to the fact that the desired steady-state values of input and output voltages and currents in a DC converter are constant DC values, i.e., $\dot{v}_{ij}^* = \dot{i}_{Lj}^* = \dot{i}_{L4}^* = \dot{v}_{o4}^* = 0$, the average switching functions of the PVU, WGU, MGU, and LBU can be driven respectively, as below:

$$u_j^* = \frac{i_{ij}^* - C_{ij}\dot{v}_{ij}^*}{2i_{Lj}^*} + \frac{L_j \dot{i}_{Lj}^* + v_{oj}^*}{2v_{ij}^*} = \frac{i_{ij}^*}{2i_{Lj}^*} + \frac{v_{oj}^*}{2v_{ij}^*} \cdot j = 1, 2, 3 \tag{24}$$

$$u_4^* = \frac{v_{i4}^* - L_4 \dot{i}_{L4}^*}{2v_{o4}^*} + \frac{C_{o4}\dot{v}_{o4}^* + i_{o4}^*}{2i_{L4}^*} = \frac{v_{i4}^*}{2v_{o4}^*} + \frac{i_{o4}^*}{2i_{L4}^*} \tag{25}$$

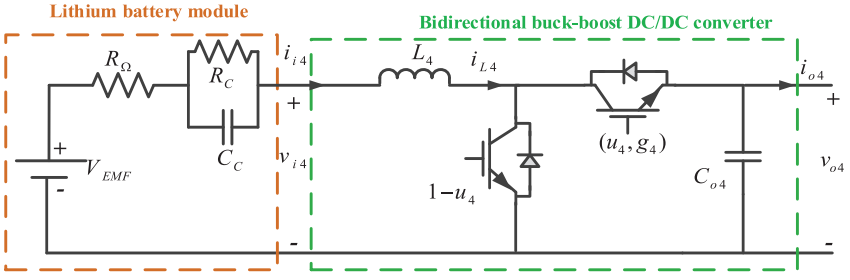

Fig. 5. The detailed structure of LBU.

It should be noticed that v_{ij}^* for $j = 1, 2, 3, 4$ are equal to the nominal input voltages of the converters, which are equal to the nominal output voltages of the DGs. Moreover, $v_{oj}^*, j = 1, 2, 3, 4$ represent the nominal output voltages of the converters, which are equal to the nominal voltage of the DC-bus v_{DC-bus}^*. Since $\dot{v}_{ij}^*$ and $\dot{v}_{oj}^*$ in Figs. 2-4 are zero, the desired values for the output capacitor currents of the buck converters are zero (which are equal to the capacitors average currents) [34]. Consequently, based on Kirchhoff's current law (KCL), the reference currents of the output inductors are equal to the desired output currents $i_{Lj}^* = i_{oj}^*$. Furthermore, as shown in Fig. 5, the current of the input inductor is equal to the desired input current $i_{L4}^* = i_{i4}^*$. The desired values of the output currents of the converters $i_{oj}^*, j = 1, 2, 3, 4$ are explained in the next subsection. Finally, the desired values $i_{ij}^*, j = 1, 2, 3, 4$ are calculated from i_{oj}^* based on equality of input and output powers of the system.

In addition, using these desired values u_j^* is calculated as the average (steady-state) component of the switching function neglecting any dynamic component. Then, the dynamic effects of state variables' errors due to the input and output fluctuations and switching effects are calculated. Finally, the modified value of the switching function is calculated.

3.2. Stability Analysis of the Generation Units

In order to investigate the dynamic stability of (8)-(10) and (14)-(16), which represent the dynamics of the PMSGs connected to the WGU and MGU respectively, we utilize IOL technique [35] in this subsection.

By considering $x_w = [i_{dw} \;\; i_{qw} \;\; \omega_{ew}]^T$, $y_w = \omega_{ew}$, and $u_w = T_{tw}$, we can rewrite the dynamics of WGU in (8)-(9) as the following form of nonlinear SISO systems:

$$\begin{aligned} \dot{x}_w &= f_w(x_w) + g_w(x_w)u_w \\ y_w &= h_w(x_w) \end{aligned} \tag{26}$$

where the vector functions f_w, g_w and the scalar fuction h_w are defined as follows:

$$f_w(x_w) = \begin{bmatrix} -a_w x_{1w} + x_{w2}x_{w3} \\ -a_w x_{w2} - x_{w1}x_{w3} - b_w x_{w3} \\ -c_w x_{w2} \end{bmatrix}, g_w(x_w) = \begin{bmatrix} 0 \\ 0 \\ \gamma_w \end{bmatrix}, h_w(x_w) = x_{w3} \tag{27}$$

where $a_w = R_{eqw}/L_{eqw}$, $b_w = \varphi_{mw}/L_{eqw}$, $c_w = 3p_w^2\varphi_{mw}/2J_w$ and $\gamma = p_w/J_w$ are positive parameters.

Based on IOL [35], by differentiating the output function until the input u_w appears, we can design u_w to cancel nonlinearity. The number r_w of differentiation required for the input u_w to appear is called the relative degree of the system. For this system, $\dot{y}_w = \dot{x}_{w3} = -c_w x_{w2} + \gamma_w u_w$, and thereby $r_w = 1$. Thus, according to IOL, we can write:

$$\dot{y}_w = (\nabla h_w)f_w + (\nabla h_w)g_w u_w \tag{28}$$

where $\nabla = \{\partial/\partial x_{w1}, \partial/\partial x_{w2}, \partial/\partial x_{w3}\}$ is the gradient operator. Therefore, if $(\nabla h_w)g_w \neq 0$, for some x_w in a finite neighborhood Ω_{x_w}, then the follow input can be written in Ω_{x_w} [35]:

$$u_w = \frac{1}{(\nabla h_w)g_w}[-(\nabla h_w)f_w + v_w] \tag{29}$$

which results in linear relation between y_w and the new input v_w namely $\dot{y}_w = v_w$. For this system:

$$\begin{aligned} (\nabla h_w)g_w &= [0 \;\; 0 \;\; 1]\begin{bmatrix} 0 \\ 0 \\ \gamma_w \end{bmatrix} = \gamma_w, (\nabla h_w)f_w \\ &= [0 \;\; 0 \;\; 1]\begin{bmatrix} -a_w x_{w1} + x_{w2}x_{w3} \\ -a_w x_{w2} - x_{w1}x_{w3} - b_w x_{w3} \\ -c_w x_{w2} \end{bmatrix} = -c_w x_{w2} \end{aligned} \tag{30}$$

Therefore, we have:

$$u_w = \frac{1}{\gamma_w}[v_w + cx_{w2}] \tag{31}$$

For the traking purpose, we can define v_w as below:

$$v_w = \dot{y}_w^* - k_w e_w \tag{32}$$

where y_w^* is the desired output, $e_w = y_w - y_w^*$ is the tracking error and k_w is a positive constant. Therefore, by replacing (32) into (31), and then rewriting $\dot{y}_w$,we have:

$$\dot{y}_w = -c_w x_{w2} + \gamma_w u_w = [y_w^* - k_w e_w] \tag{33}$$

Thus, the tracking error of the closed loop system becomes $\dot{e}_w + k_w e_w = 0$ which represent an asymptotially stable error dynamics and the tracking error converges to zero asymptotially. However, this accounts for only a part of the closed-loop dynamics related to $y_w = x_{w3}$ while the system (26) has order 3. Therefore, there is an internal dynamics related to x_{w1} and x_{w2} which has not been observed by IOL. If this internal dynamics is stable, our tracking control problem has been solved. The study of the internal dynamics stability can be simplified locally by studying that of the zero-dynamics instead. The zero dynamic is defined to be the internal dynamics when the system output is kept zero [35]. We have the following theorem:

Theorem 1. [35]. Assume that the system (26) has relative degree r_w, and that its zero dynamics is asymptotically stable. Choose constants k_w such that the polynomial $\dot{e}_w + k_w e_w = 0$ has all its roots strictly in the left-half plane. Then, the control law (31) yields a locally asymptotically stable closed-loop system.

Based on IOL, the system (26) can be transformed to a normal form if there exist the following diffeomorphism [35]:

$$\phi_w(x) = [\mu_{w1} \;\; \psi_{w1} \;\; \psi_{w2}] \tag{34}$$

where $\mu_{w1} = y_w$, and ψ_{w1} and ψ_{w2} are related to the internal dynamics and they are chosen so that $(\nabla\psi_{w1})g_w = 0$ and $(\nabla\psi_{w2})g_w = 0$. By choosing $\psi_{w1} = x_{w1}$ and $\psi_{w2} = x_{w2}$, the system dynamics is put into the following normal form:

$$\begin{aligned} \dot{\psi}_{w1} &= -a_w\psi_{w1} + \psi_{w2}\mu_{w1} \\ \dot{\psi}_{w2} &= -a_w\psi_{w2} - \psi_{w1}\mu_{w3} - b_w\mu_{w1} \\ \dot{\mu}_{w1} &= c_w\psi_{w2} + \gamma_w u \end{aligned} \tag{35}$$

The internal dynaimcs is:

$$\begin{aligned} \dot{x}_{w1} &= -a_w x_{w1} + x_{w2}x_{w3} \\ \dot{x}_{w2} &= -a_w x_{w2} - x_{w1}x_{w3} - b_w x_{w3} \end{aligned} \tag{36}$$

Therefore, the zero dynamics becomes:

$$\begin{aligned} \dot{x}_{w1} &= -a_w x_{w1} \\ \dot{x}_{w2} &= -a_w x_{w2} \end{aligned} \tag{37}$$

The above zero dynamics is asymptotically stable for $a_w > 0$. Thus, the control law (31) can locally asymptotically stabilize the nonlinear system (26).

As a result, for the system of (8)-(9), if the following relation holds, the system will be stable:

$$T_{tw} = \frac{J_w}{p_w}\left[\dot{\omega}_{ew}^* - k_w(\omega_{ew} - \omega_{ew}^*) + \frac{3p_w^2\varphi_{mw}}{2J_w}i_{dw}\right] \tag{38}$$

Similar results can be obtained for the dynamics of MGU in (14)-(16), by replacing the subscript '*w*' to '*m*' in the equations of (26)-(38).

3.3. DLM-based Controller of the Converters and Stability Analysis

DLM is aimed to stabilize the state variables of the DC-DC converters in the considered DC micro-grid in Fig. 1, such that the output currents and the DC-bus voltage reach their equilibrium points. In this way the

output varriables of the micro-grid have a stable operation in both steady-state and dynamic conditions. The error variables of the converters can be written as:

$$E = [e_1 \;\; e_2 \;\; e_3 \;\; e_4 \;\; e_5 \;\; e_6 \;\; e_7 \;\; e_8]^T = [v_{i1} \;\; i_{L1} \;\; v_{i2} \;\; i_{L2} \;\; v_{i3} \;\; i_{L3} \;\; i_{L4} \;\; v_{DC-bus}] - [v_{i1}^* \;\; i_{L1}^* \;\; v_{i2}^* \;\; i_{L2}^* \;\; v_{i3}^* \;\; i_{L3}^* \;\; i_{L4}^* \;\; v_{DC-bus}^*] \tag{39}$$

where E is the vector of the errors and $(v_{DC-bus}, v_{DC-bus}^*) = (v_{oj}, v_{oj}^*)$, $j = 1, 2, 3, 4$, represents the DC-bus voltage and its reference value. In order to stabilize the error vaiables of the all converters and control their output variables, the proper Lyapunov candidate $V(E)$ is described by:

$$V(E) = \frac{1}{2} tr[diag(B).\, diag(E)^2] \tag{40}$$

where B is the parameter vector defined as $B = [C_{i1} \;\; L_1 \;\; J_w \;\; C_{i2} \;\; L_2 \;\; J_m \;\; C_{i3} \;\; L_3 \;\; L_4 \;\; 4C_o]^T$. Moreover, it is assumed that $C_{o1} = C_{o2} = C_{o3} = C_{o4} = C_o$. According to DLM, in order to reach the asymptotical stability, $V(E)$ must be positive and its derivative must be definitely negative, that is [35]:

$$\begin{cases} V(0) = 0 \\ V(E) \succ 0, \;\; \forall\, E \neq 0 \\ \dot{V}(E) \prec 0, \forall\, E \neq 0 \end{cases} \tag{41}$$

where x denotes the variables represented in (39). Based on (41), it is obvious that $V(0) = 0$, $V(E) > 0$ for all $E \neq 0$. By making time derivative of $V(E)$, we have:

$$\dot{V}(E) = tr[diag(B).\, diag(E).\, diag(\dot{E})] \tag{42}$$

The switching functions of the used converters in the energy-management-based control system are defined as:

$$u_j = u_j^* - U_j \quad , \quad j = 1, 2, 3, 4 \tag{43}$$

where $U_j$is the dynamic part of the switching functions. By applying (39) and (43) to equations (5)-(7), (11)-(13), (17)-(19) and (21), (22) all terms of (42) can be achieved as:

$$\begin{cases} C_{i1} e_1 \dot{e}_1 = (i_{i1} - i_{i1}^*) e_1 - (e_2 u_1 - i_{L1}^* U_1) e_1 \\ C_{i2} e_3 \dot{e}_3 = (i_{i2} - i_{i2}^*) e_3 - (e_4 u_2 - i_{L2}^* U_2) e_3 \\ C_{i3} e_5 \dot{e}_5 = (i_{i3} - i_{i3}^*) e_5 - (e_6 u_3 - i_{L3}^* U_3) e_5 \\ 4C_o e_8 \dot{e}_8 = e_7 u_4 e_8 - e_8 U_4 i_{L4}^* - e_8 \sum_{j=1}^{4} (i_{oj} - i_{oj}^*) + e_8 e_2 + e_4 e_8 + e_6 e_8 \end{cases} \tag{44a}$$

$$\begin{cases} L_1 e_2 \dot{e}_2 = (e_1 u_1 - v_{i1}^* U_1) e_2 - e_2 e_8 \\ L_2 e_4 \dot{e}_4 = (e_3 u_2 - v_{i2}^* U_2) e_4 - e_8 e_4 \\ L_3 e_6 \dot{e}_6 = (e_7 u_3 - v_{i3}^* U_3) e_6 - e_8 e_6 \\ L_4 e_7 \dot{e}_7 = (v_{i4} - v_{i4}^*) e_7 - e_7 u_4 e_8 + e_7 U_4 v_{DC-bus}^* \end{cases} \tag{44b}$$

By substituting (44) into (42), and after simplifying the equation, the derivative of $V(E)$ can be obtiained as:

$$\begin{aligned} \dot{V}(E) = {} & [(i_{i1} - i_{i1}^*) + i_{L1}^* U_1] e_1 - (e_2 v_{i1}^*) U_1 + [(i_{i2} - i_{i2}^*) + i_{L2}^* U_2] e_3 \\ & - (e_4 v_{i2}^*) U_2 \\ & + [(i_{i3} - i_{i3}^*) + i_{L3}^* U_3] e_5 - (e_6 v_{i3}^*) U_3 + [(v_{i4} - v_{i4}^*) + U_4 v_{DC-bus}^*] e_7 \\ & - e_8 \left[U_4 i_{L4}^* + \sum_{j=1}^{4} (i_{oj} - i_{oj}^*) \right] \end{aligned} \tag{45}$$

To reach the asymptotic stability, it has to be proven that $\dot{V}(E) \prec 0$ for all $E \neq 0$. In the equation above, we assume that the values of the terms associated with each converter are negative, accordingly the sum of the equations (45) will be negative in the situation of participation of all or some of the resources. On this basis, we can state the following theorem:

Theorem 2. . In a system with the Lyapunov function defined by (40), considering the relation (45), if there exist negative factors $\alpha_1, \alpha_2, \alpha_3, \alpha_4$ such that $\frac{\alpha_j e_{kj} - (i_{ij} - i_{ij}^*)}{e_{kj+1}} > 0$ for $j = 1, 2, 3$ and $\frac{\alpha_4 e_{k4} - (v_{i4} - v_{i4}^*)}{e_{k4+1}} > 0$ where $[k_1, k_2, k_3, k_4] = [1, 3, 5, 7]$ then there are U_j for $j = 1, 2, 3, 4$ described by (46)-(49) making the system asymptotically stable according to the Lyapunov definition.

$$U_1 = \frac{\alpha_1 e_1 - (i_{i1} - i_{i1}^*)}{i_{L1}^*} \tag{46}$$

$$U_2 = \frac{\alpha_2 e_3 - (i_{i2} - i_{i2}^*)}{i_{L2}^*} \tag{47}$$

$$U_3 = \frac{\alpha_3 e_5 - (i_{i3} - i_{i3}^*)}{i_{L3}^*} \tag{48}$$

$$U_4 = \frac{\alpha_4 e_7 - (v_{i4} - v_{i4}^*)}{v_{DC-bus}^*} \tag{49}$$

Proof. . At first, we consider two first terms in (45), i.e., $\dot{V}_1 := [(i_{i1} - i_{i1}^*) + i_{L1}^* U_1] e_1 - (e_2 v_{i1}^*) U_1$. By replacing (46) into $\dot{V}_1$, we have:

$$\dot{V}_1 := \alpha_1 e_1^2 - \frac{1}{i_{L1}^* v_{i1}^*} \left[\frac{\alpha_1 e_1 - (i_{i1} - i_{i1}^*)}{e_2} \right] (e_2 v_{i1}^*)^2 \tag{50}$$

Since, the references i_{L1}^* and v_{i1}^* are positive values and also, as assumed in the theorem hypothesis, there exist $\alpha_1 < 0$ and $\frac{\alpha_1 e_1 - (i_{i1} - i_{i1}^*)}{e_2} > 0$, thus, we can write that $\dot{V}_1 < 0$.

Similarly, by replacing the equations (47)-(49) into the remaining parts of (45), using the same proof, it can also be proven that the remaining parts of $\dot{V}$ are also negative. Therefore, the system is asymptotically stable.

Remark 1. . It should be noticed that the assumptions in the hypothesis of Theorem 2 are physically feasible. For a given input power of converter (P_{in}), an increase in current causes the decrease in the voltage, since the reference and the actual currents are $i_{i1}^* = P_{in}/v_{i1}^*$ and $i_{i1} = P_{in}/v_{i1}$ respectively. Therefore, the sign of e_1 is always opposite of the sign of $(i_{i1} - i_{i1}^*)$. Knowing this fact and by investigating all possible signs of e_1 and e_2, it can be said that it is always possible to find

Table 1
Considering the feasibility of the inequality related to Remark 1 under various conditions.

Sign of (e_1)	Sign of($i_{i1} - i_{i1}^*$)	Sign of (e_2)	Equation analysis
+	-	+	$\alpha_1 e_1 - (i_{i1} - i_{i1}^*) > 0 \Rightarrow \alpha_1 > \frac{(i_{i1} - i_{i1}^*)}{e_1} \Rightarrow \frac{(i_{i1} - i_{i1}^*)}{e_1} < \alpha_1 < 0$
+	-	-	$\alpha_1 e_1 - (i_{i1} - i_{i1}^*) < 0 \Rightarrow \alpha_1 < \frac{(i_{i1} - i_{i1}^*)}{e_1}$
-	+	+	$\alpha_1 e_1 - (i_{i1} - i_{i1}^*) > 0 \Rightarrow \alpha_1 < \frac{(i_{i1} - i_{i1}^*)}{e_1}$
-	+	-	$\alpha_1 e_1 - (i_{i1} - i_{i1}^*) < 0 \Rightarrow \alpha_1 > \frac{(i_{i1} - i_{i1}^*)}{e_1} \Rightarrow \frac{(i_{i1} - i_{i1}^*)}{e_1} < \alpha_1 < 0$

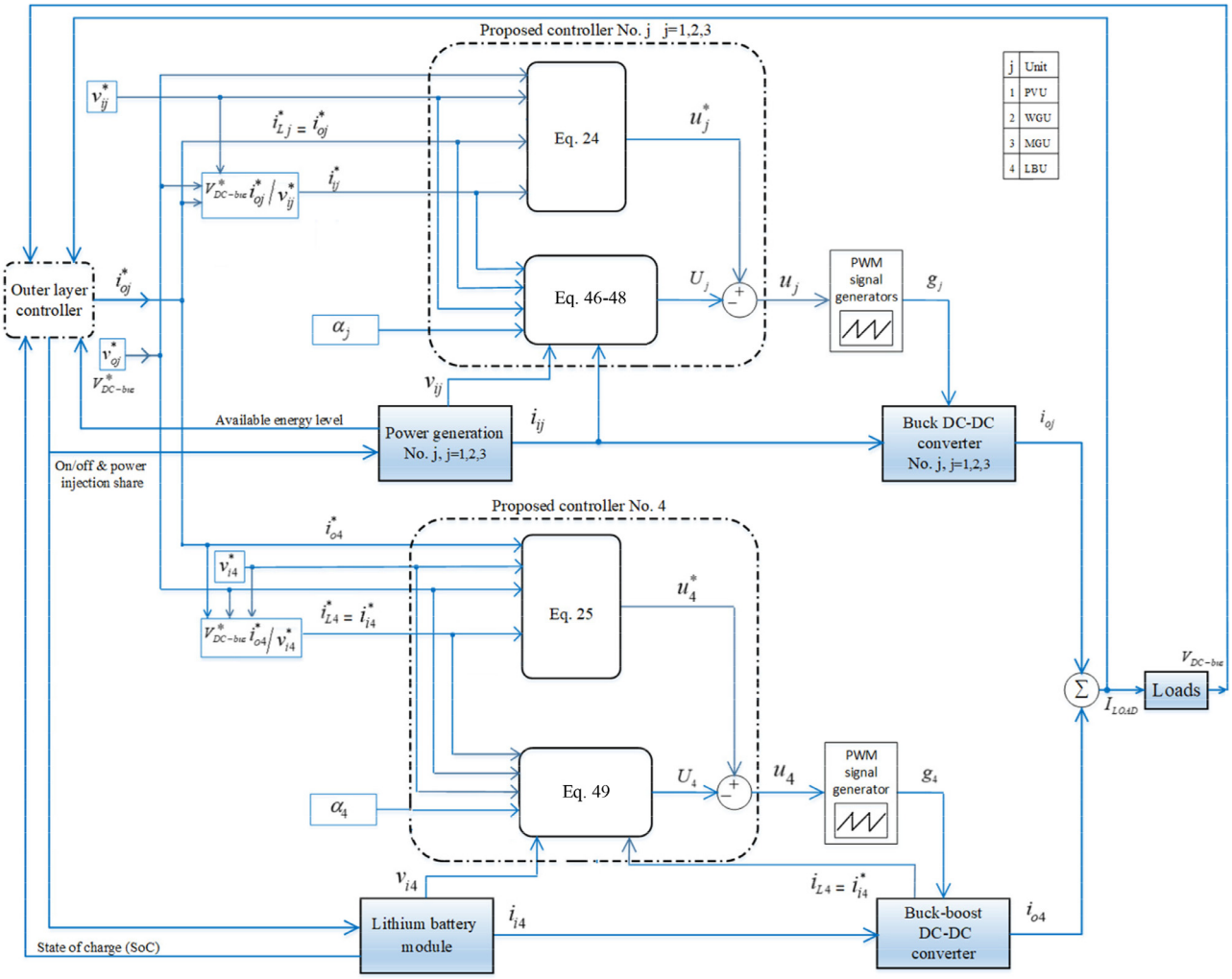

Fig. 6. The detailed structure of the proposed control technique.

$\alpha_1 < 0$ such that satisfies $\frac{\alpha_1 e_1 - (i_{l1} - i_{l1}^*)}{e_2} > 0$. The feasibility of this inequality has been studied under various conditions in Table 1.

As can be seen, the mentioned inequality is feasible under the various condition and there are always negative boundaries for α_1.

In this paper, the control variables are the switching functions of the DC/DC converters (u_j). After separating the steady-state and dynamic components of the switching functions (u_j^*, U_j), in order to ensure the system stability and eliminate the effects of the dynamics of the state-space variables errors, the DLM is applied, and then the dynamic components of the switching functions (U_j) are calculated. After removing the effect of the dynamic components of the switching function from the average switching function (u_j^*), the modified switching functions ($u_j = u_j^* - U_j$) are applied to the pulse width modulation (PWM) signal generator as control commands and the switching signals (g_j) are exported and applied to the converters. Consequently, the output currents of the converters are regulated with acceptable accuracy, swift transient-state, and insignificant steady-state oscillations. These features stabilize the DC-bus voltage in various conditions of the micro-grid operation.

The detailed structure of the proposed controller is shown in Fig. 6. As can be seen from this figure, the proposed switching functions consist of all the state variables errors and the dynamic factors can highly affect the proposed controller operation. All the power generation units, controllers, equations and variables, along with their relationships, are shown in Fig. 6. In this figure, V_{DC-bus} is the DC-bus voltage that is equal to the load voltage, and I_{LOAD}, is the total load current. The load in this paper is considered as a linear resistive DC load. The outer layer controller in this paper is based on the strategy presented in [8], which determines the contribution of each generation unit according to the load consumption and availability of the energy level such as solar radiation and wind speed rate and considering the state of charge (SoC) of the battery. This contribution level is applied to the proposed controllers as a reference current signal (i_{oj}^*). Moreover, in some cases; during a severe load decrement, it may be necessary that one or two power generation units be turned off. The outer layer controller is responsible for specifying the reference values (i_{oj}^*) for the output current of each converter in the considered DC micro-grid. Indeed, the task of the proposed controller is the regulation of the output current of the converters, based on the calculated reference of (i_{oj}^*) aimed to decrease the dynamic fluctuations and reaching acceptable accuracy and smooth voltage, regardless of this fact that which method is used in the outer layer controller. Obviously, the reference values (i_{o1}^*) for the PVU and (i_{o2}^*) for the WGU have been determined by the outer layer controller based on the available energy of the solar irradiation and the wind speed. The reference value of the output current of the WGU (i_{o3}^*) is set in order to compensate for the significant reduction in the renewable energy generation units and the reference value of the output current of the LBU (i_{o4}^*) is adjusted based on the difference between the total generated current and the reference value of the load current $i_{o4}^* = I_{LOAD}^* - \sum_{j=1}^{3} i_{oj}$. In this way, the errors of the generated currents are compensated by the LBU. Considering the linear resistive load, instantaneous detection of the load is carried out by

$R_{LOAD} = v_{DC-bus}/I_{LOAD}$. Then, through the relationship $I^*_{LOAD} = (v^*_{DC-bus}/v_{DC-bus})$. I_{LOAD}, the reference value of the total current of the load can be calculated.

In practice, if $P_{wind} + P_{pv} < P_{Load}$, both WGU and PVU are set at the maximum power generation and the rest of the needed power is supplied through the controllable resources such as LBU and MGU. Also, where the generation of PVU or WGU is more than the needed load power, LBU operates in charging-mode ($i^*_{o4} < 0$) in order to balance the power and stabilize the DC-bus voltage subsequently.

As it is discussed in this paper, regulating the DC-bus voltage should be accomplished accurately. To analyze the operation of the proposed control technique based on the dynamic models, firstly the relationships between the output voltage of the DC/DC converters and its switching functions are calculated. Considering the output voltage dynamic of the converters in (7), (13), (19) and (22), the relationships for the buck and buck-boost converters, can be driven as (51) and (52) respectively:

$$\frac{dv_{oj}}{dt} = \frac{1}{C_{oj}}\left(\frac{C_{ij}\frac{dv_{ij}}{dt} - i_{ij}}{U_j - u^*_j}\right) - \frac{i_{oj}}{C_{oj}} \quad ,(j = 1, 2, 3) \tag{51}$$

$$\frac{dv_{o4}}{dt} = -\frac{i_{L4}}{C_{o4}}U_4 + \left(\frac{i_{L4}}{C_{o4}}u^*_4 - \frac{i_{o4}}{C_{o4}}\right) \tag{52}$$

Based on (51) and (52), two diagrams associated with the derivatives of output voltages of buck and buck-boost DC/DC converters are drawn in Fig. 7.a and 7.b respectively.

Fig. 7 has been presented to show how the dynamic parts of the proposed control technique can impact on the dynamic of the output voltages of all DC/DC converters. In order to have a desired DC-link voltage with slight fluctuations, all buck, and bidirectional buck-boost DC/DC converters must generate desired DC-link voltage in its output. This issue is evaluated in this part. It can be realized from Fig. 7.a that when the dynamic part $U_j$is increased, a constant value is achieved for dv_{oj}/dt. For a suitable operating condition, the term dv_{oj}/dt must be zero that happens in the point near to $U_j = u_j*$ as depicted in Fig. 7.a. In contrast, for bidirectional buck-boost DC/DC converter, the zero value is obtained for dv_{o4}/dt, when the following relation is governed for U_4,

$$U_4 = \left(u^*_4 - \frac{i_{o4}}{i_{L4}}\right) \tag{53}$$

Using (53), the curve of dv_{o4}/dt based on U_4 is illustrated in Fig. 7.b. For a suitable operation of the proposed control technique, the switching functions dynamics and derivative of the output voltages must be zero. In this condition, the output currents will be equal to:

$$i_{oj} = -\left(\frac{C_{ij}\frac{dv_{ij}}{dt} - i_{ij}}{u^*_j}\right) \quad ,(j = 1, 2, 3) \tag{54}$$

$$i_{o4} = u^*_4 i_{L4} \tag{55}$$

As can be seen in (54), in addition to the steady-state of switching functions, the output currents of the buck converters depend on the input currents and voltages. For the bidirectional buck-boost DC/DC converter, the output current is affected by the filter inductance current as well as the steady-state switching function as can be observed in (55).

4. Simulation and Results

In this section, the proposed control technique is evaluated in MATLAB/SIMULINK environment. Three scenarios are specified based on verifying the ability of the proposed controller at accurate tracking of converters currents, DC-bus voltage regulation and the reduction of output currents fluctuations during the steady-state and transient variations of the loads and input power changes of the generation resources. In the first scenario, two loads are abruptly connected to DC-bus at t = 1s. In this condition, LBU is immediately set to compensate for this load variation. In addition, at t = 1.75s a simultaneous change in load and PVU generation occurs. The changes in the load during the simulation are implemented as changes in the load resistance. In the second scenario, firstly a load increment happens at t = 2.5s that is supplied by WGU. Moreover, the WGU speed decreases at t = 3.25s and the MGU operates immediately to provide the lack of the DC power demand. Finally, in the third scenario, a severe load decrement happens at t = 5s. In this condition, power generation decreases and even the lithium battery is utilized to balance the power. The simulation parameters are given in Table 2.

4.1. Scenario I: LBU and PVU operation assessment

In this sub-section, all units are in power generation mode. In addition to supplying a DC load increment at t = 1s, LB-based bidirectional DC/DC converter must compensate for the current fluctuations. The DC-bus voltage, total load current and the output current of each generation unit during the first scenario are given in Figs. 8-10, respectively. As it can be seen from Fig. 10, the generation units are able to inject the needed currents of the DC loads in steady-state and reach the desired value for DC-bus voltage with negligible undershoot. The DC load variations are considered according to Fig. 9. After a load change at t = 1s, LBU output current increases with a good transient time as shown in Fig. 10. Also, a simultaneous load and generation power

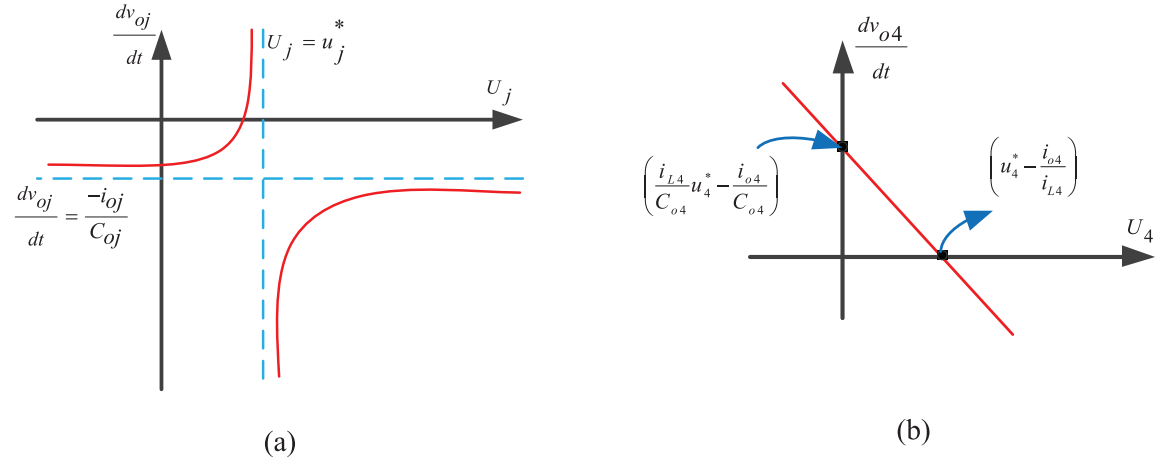

Fig. 7. The derivatives of output voltages of (a) buck, and (b) buck-boost DC/DC converters.

Table 2
The parameters of the proposed system.

Parameters		Value	Parameters		Value
DC-bus	Reference voltage (V)	950	All converters	Input reference voltages (V)	1400
Buck DC/DC converter	Inductance (mH)	3	Buck-boost DC/DC converter	Inductance (mH)	3
	Output capacitance (μF)	20		Output capacitance (μF)	20
	Input capacitance (mF)	0.1	DC Load power	Min (kW)	11.4
Switching	Frequency (kHz)	5		Max (kW)	52.25

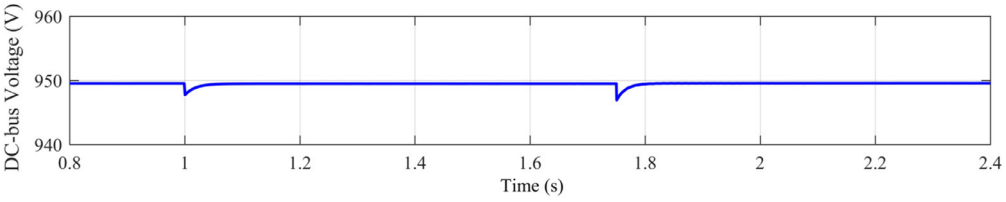

Fig. 8. DC-bus voltage under load changes during scenario I.

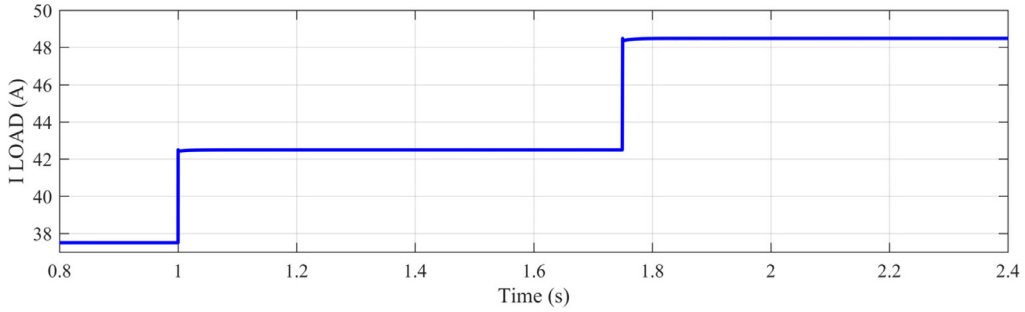

Fig. 9. Total load current during scenario I.

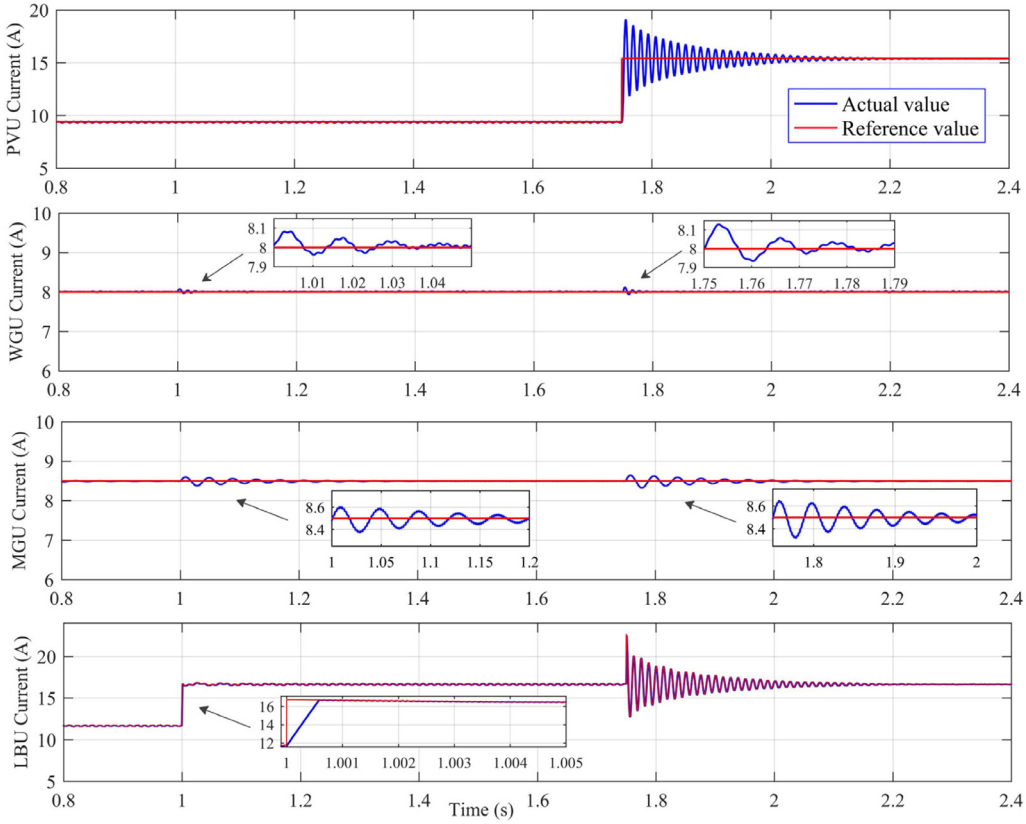

Fig. 10. The output currents of each generation unit under load change and the wind speed decrement during scenario I.

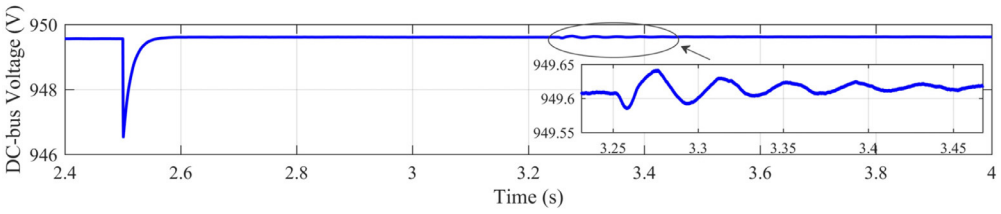

Fig. 11. DC-bus voltage under load change and the wind speed decrement during scenario II.

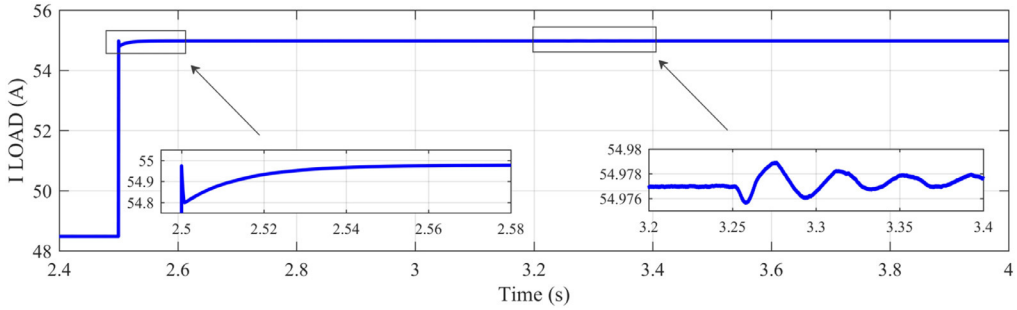

Fig. 12. Total load current during scenario II.

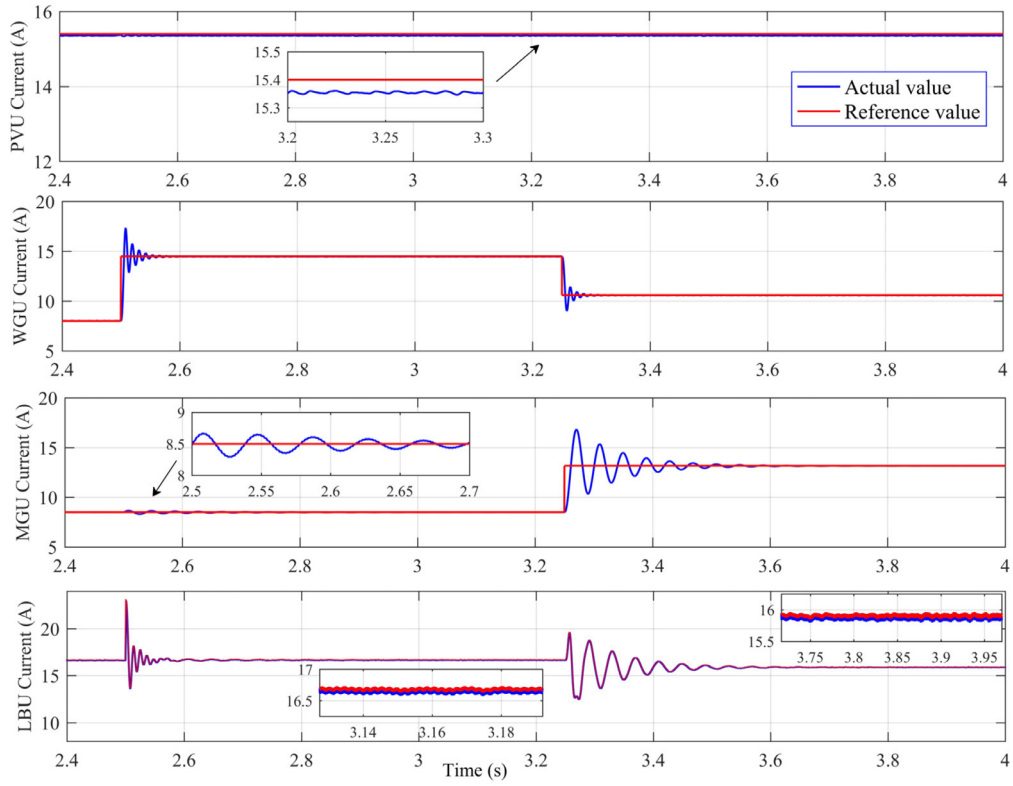

Fig. 13. The output currents of each generation unit under load change and the wind speed decrement during scenario II.

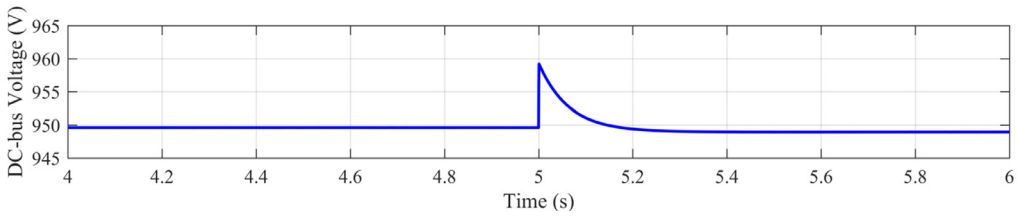

Fig. 14. DC-bus voltage under severe load decrement at t = 5 s during scenario III.

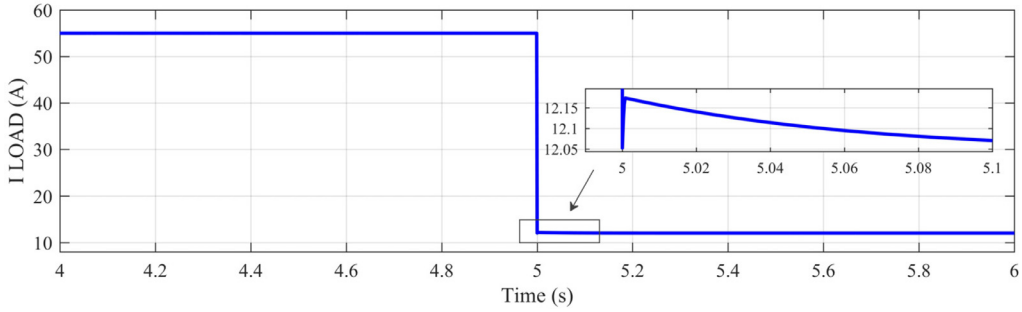

Fig. 15. A severe load decrement at t = 5 s during scenario III.

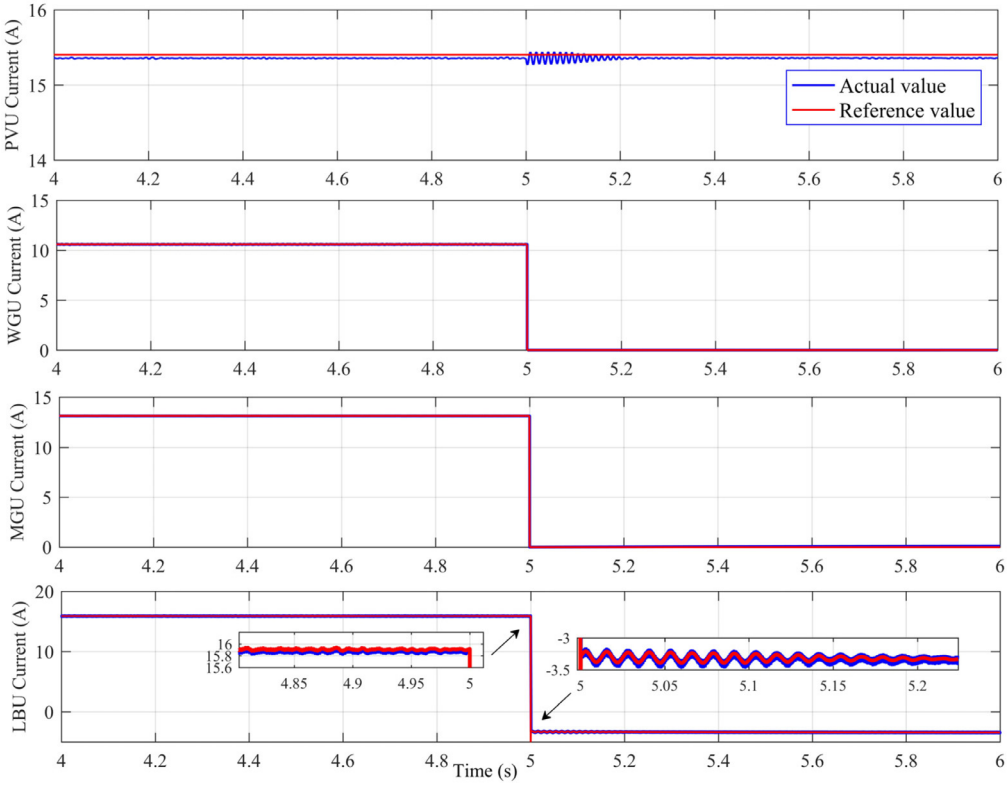

Fig. 16. The output currents of each generation unit under severe load decrement at t = 5 s in scenario III.

Table 3
The summary of the events, system reactions and their results in simulation.

Scenario	Time (s)	Events	System reactions	$I_{LOAD\text{-}ss}$ (A)	$V_{DC\text{-}bus\text{-}ss}$ (V)	$e_{v\text{-}ss}$ %
Scenario I	1	Load↑	LBU↑ (discharging)	42.502	949.62	0.04
	1.75	Load↑ & PVU↑	LBU↓ (discharging)	48.494	949.67	0.034
Scenario II	2.5	Load↑	WGU↑	54.982	949.70	0.031
	3.25	WGU↓	MGU↑	54.983	949.71	0.030
Scenario III	5	Load↓↓	~~MGU~~, ~~WGU~~, LBU↓ (charging)	12.053	949.72	0.029

increment occurred at t = 1.75s. With the aim of DC-bus voltage stabilization, the reference current of LBU is set to compensate for the current fluctuations due to other units which is executed carefully according to Fig. 10. Also, the other generation units can provide desired output currents during the first scenario with good steady-state responses. It leads to a desired constant value for the DC-bus voltage with an acceptable transient response as depicted in Fig. 8. Consequently, Figs. 8-10 verify that the proposed control strategy can accurately specify the duties of PV and LB-based DC/DC converters to stabilize the DC-bus voltage with a swift response, perform a very good current tracking and decrease the output currents fluctuations in both steady and transient responses.

4.2. Scenario II: WGU and MGU operation assessment

In this sub-section, the performances of The WGU, MGU, and LBU are evaluated to determine the proposed control technique ability at executing the accurate current tracking, providing stable DC-bus voltage and reducing the output currents fluctuations. When a load is connected to the DC-bus at t = 2.5s, the output current reference of the WGU-based converter is immediately increased to extract the needed current and inject to the DC-bus as depicted in Fig. 13.

According to Fig. 13, the generated fluctuations at t = 2.5s is completely compensated by LBU leading to stable DC-bus voltage and smooth load current as depicted in Fig. 11 and 12, respectively. Moreover, the wind speed of WGU decreases at t = 3.25s that leads to a decrement at injecting the DC current according to Fig. 13. In this condition, the MGU is adjusted to generate more output current as shown in Fig. 13. Based on this figure, since increasing the generated power of the MGU is more than load demand, it is imperative to reduce the power injected by the LBU. In addition, at t = 3.25, the fluctuations are completely produced by LBU. It leads to DC-bus voltage stability with a slight transient response during the wind speed decrement and an accurate current tracking as depicted in Fig. 11 and 12, respectively.

4.3. Scenario III: Severe load decrement

In this subsection, the proposed control strategy is aimed to provide the bidirectional operation for LB-based DC/DC converter to inverse the current flow into the considered battery. For this purpose, the severe load decrement shown in Fig. 15 is carried out. The output currents of each unit are depicted in Fig. 16. According to this load change, the output currents of WGU and MGU are set to reach zero. Because of severe load decrement shown in Fig. 15, there is no need for the output currents of WGU and MGU anymore. In another side, PVU is set to keep its generated output current constant as shown in Fig. 16. This figure shows that the proposed control strategy is able to enforce a constant current generation algorithm for PVU under severe load variation. The LBU output current can be seen from Fig. 15. According to this figure, inversed current flow can be completely performed by the help of applying the proposed control technique to LBU with very good steady and transient conditions. The DC-bus voltage in this condition is illustrated in Fig. 14. Based on this figure, the DC-bus voltage stabilization can be accurately done even under severe load decrement. For this subsection, it can be said that proposed controller strategy can easily provide inversed current flow for LBU and constant current generation for PVU under severe load change in which both DC-bus voltage and DC load currents appropriately approaches their desired values.

A summary of the events, system reactions and their results are shown in Table 3. In this table. $I_{LOAD\text{-}ss}$, is the steady-state current of the load, $V_{DC\text{-}bus\text{-}ss}$ the steady-state voltage of the DC-bus that is equal to the load voltage. The $e_{v\text{-}ss}$% is the steady-state error of the DC-bus voltage, expressed as a percentage.

5. Conclusion

In this paper, a scheme of DC-bus voltage regulation of a stand-alone DC micro-grid consisting of PVU, WGU, MGU, and LBU have been proposed to provide a controller, based on DLM under variations of load and power generation. For this, a comprehensive dynamic model associated with the power converters of an energy storage system and all generation units has been considered. In the proposed method, both steady-state and dynamic conditions have been investigated in the dynamic model in order to decrease the fluctuations due to the load alterations and performance of the generation units. The main advantages of this control technique are the generation of separate components for the dynamic parts of the converter switching functions as well as employing all dynamic zeros of converter-based equations, simplicity, easy execution, and the least need for communications between the controllers. Desired DC-bus voltage, accurate current generation and supplying the load appropriately with fast dynamic responses have been achieved by the proposed controller performance in the MATLAB/Simulink environment for various operating conditions. Moreover, the simulation results and examining equations (24), (25) and (46)-(48) show that the generated currents of PVU, WGU, and MGU are controlled individually and their effects on each other are negligible. In addition, all the aforementioned advantages cause to reduce the stresses on the LBU and increase the battery life-span. It can be predicted that achieving the dynamic factors of proposed control technique through a supplementary closed loop-based controller as well as considering the errors dynamic of mechanical state variables will improve significantly the convergence rate and transient responses of DC/DC converters state variables. Also, in this condition, combining an adaptive controller with proposed Lyapunov controller and proposing a method for the practical implementation of mechanical torque controller in stand-alone micro-grids based on IOL can be considered as future works.

Author Contribution

Arash Abedi: Methodology, Software, Writing - Original Draft

Behrooz Rezaie: Conceptualization, Formal analysis, Investigation, Writing - Review & Editing, Supervision

Alireza Khosravi: Investigation, Writing - Review & Editing, Supervision

Majid Shahabi: Investigation, Writing - Review & Editing, Supervision

Decleration of competing Interest

None

References

[1] W Alharbi, K. Raahemifar, Probabilistic coordination of microgrid energy resources operation considering uncertainties, Electric Power Syst. Res. 128 (2015) 1–10.
[2] A.T. Elsayed, A.A. Mohamed, O.A. Mohammed, *DC microgrids and distribution systems: an overview*, Electr. Power Syst. Res. 119 (2015) 407–417.
[3] M Mehrasa, et al., A control plan for the stable operation of microgrids during grid-connected and islanded modes, Electr. Power Syst. Res. 129 (2015) 10–22.
[4] Z. Wang, B. Chen, J. Wang, Decentralized energy management system for networked microgrids in grid-connected and islanded modes, IEEE Trans. Smart Grid 7 (2) (2016) 1097–1105.
[5] E. Pouresmaeil, M. Mehrasa, J.P. Catalão, A multifunction control strategy for the stable operation of DG units in smart grids, IEEE Trans. Smart Grid 6 (2) (2015) 598–607.
[6] C. Chakraborty, H.H.-C. Iu, D.D.-C. Lu, Power converters, control, and energy management for distributed generation, IEEE Trans. Ind. Electron. 62 (7) (2015) 4466–4470.
[7] M.J Rana, M.A. Abido, Energy management in DC microgrid with energy storage and model predictive controlled AC–DC converter, IET Gen. Transm. Distrib. 11 (15) (2017) 3694–3702.
[8] A. Tani, M.B. Camara, B. Dakyo, Energy management in the decentralized generation systems based on renewable energy—ultracapacitors and battery to compensate the wind/load power fluctuations, IEEE Trans. Ind. Appl. 51 (2) (2015) 1817–1827.
[9] Y. Kuang, et al., A review of renewable energy utilization in islands, Renewable Sustainable Energy Rev. 59 (2016) 504–513.
[10] Y.-S. Kim, E.-S. Kim, S.-I. Moon, Frequency and voltage control strategy of standalone microgrids with high penetration of intermittent renewable generation systems, IEEE Trans. Power Syst. 31 (1) (2016) 718–728.
[11] J. Han, S.K. Solanki, J. Solanki, Coordinated predictive control of a wind/battery microgrid system, IEEE J. Emerg. Sel. Top. Power Electron. 1 (4) (2013) 296–305.
[12] D. Chen, L. Xu, L. Yao, DC voltage variation based autonomous control of DC microgrids, IEEE Trans. Power Deliv. 28 (2) (2013) 637–648.
[13] G. Xu, et al., Coordinated DC voltage control of wind turbine with embedded energy storage system, IEEE Trans. Energy Convers. 27 (4) (2012) 1036–1045.
[14] M. Mehrasa, et al., Passivity-based control technique for integration of DG resources into the power grid, Int. J. Electr. Power Energy Syst. 58 (2014) 281–290.
[15] N Eghtedarpour, E. Farjah, Distributed charge/discharge control of energy storages in a renewable-energy-based DC micro-grid, IET Renewable Power Gen. 8 (1) (2014) 45–57.
[16] M.B. Camara, B. Dakyo, H. Gualous, Polynomial control method of DC/DC converters for DC-bus voltage and currents management—battery and supercapacitors, IEEE Trans. power Electron. 27 (3) (2012) 1455–1467.
[17] K. Sun, et al., A distributed control strategy based on DC bus signaling for modular photovoltaic generation systems with battery energy storage, IEEE Trans. Power Electron. 26 (10) (2011) 3032–3045.
[18] L Xu, D. Chen, Control and operation of a DC microgrid with variable generation and energy storage, IEEE Trans. Power Deliv. 26 (4) (2011) 2513–2522.
[19] M. Kumar, S. Srivastava, S. Singh, Control strategies of a DC microgrid for grid connected and islanded operations, IEEE Trans. Smart Grid 6 (4) (2015) 1588–1601.
[20] A Deihimi, M.E.S. Mahmoodieh, Analysis and control of battery-integrated dc/dc converters for renewable energy applications, IET Power Electron. 10 (14) (2017)

1819–1831.
[21] B Banerjee, W.W. Weaver, Generalized geometric control manifolds of power converters in a DC microgrid, IEEE Trans. Energy Convers. 29 (4) (2014) 904–912.
[22] M. Rashad, et al., Mathematical modeling and stability analysis of DC microgrid using sm hysteresis controller, Int. J. Electr. Power Energy Syst. 95 (2018) 507–522.
[23] M. Kumar, et al., Development of a new control strategy based on two revolving field theory for single-phase VCVSI integrated to DC microgrid, Int. J. Electr. Power Energy Syst. 98 (2018) 290–306.
[24] M. Baharizadeh, H.R. Karshenas, J.M. Guerrero, An improved power control strategy for hybrid AC-DC microgrids, Int. J. Electr. Power Energy Syst. 95 (2018) 364–373.
[25] N. Yang, et al., Compensation of droop control using common load condition in DC microgrids to improve voltage regulation and load sharing, Int. J. Electr. Power Energy Syst. 64 (2015) 752–760.
[26] V Mortezapour, H. Lesani, Hybrid AC/DC microgrids: a generalized approach for autonomous droop-based primary control in islanded operations, Int. J. Electr. Power Energy Syst. 93 (2017) 109–118.
[27] B.-.S. Ko, G.-.Y. Lee, K.-.Y. Choi, Rae-Young Kim, A coordinated droop control method using a virtual voltage axis for power management and voltage restoration of DC microgrids, IEEE Trans. Ind. Electron. (2018).
[28] Srikanth Kotra, K. Mishra Mahesh, Design and stability analysis of DC microgrid with hybrid energy storage system, IEEE Trans. Sustainable Energy (2019).
[29] M. Su, Z. Liu, Y. Sun, H. Han, X. Hou, Stability analysis and stabilization methods of DC microgrid with multiple parallel-connected DC–DC converters loaded by CPLs, IEEE Trans. Smart Grid 9 (1) (2018) 132–142.
[30] A.P.N. Tahim, D.J. Pagano, E. Lenz, V. Stramosk, Modeling and stability analysis of Islanded DC microgrids under droop control, IEEE Trans. Power Electron. 30 (8) (2015) 4597–4607.
[31] S. Benelghali, et al., Experimental validation of a marine current turbine simulator: application to a PMSG-based system second-order sliding mode control, IEEE Trans. Ind. Electron. 58 (1) (2011) 118–126.
[32] H. Shariatpanah, R. Fadaeinedjad, M. Rashidinejad, A new model for PMSG-based wind turbine with yaw control, IEEE Trans. Energy Convers. 28 (4) (2013) 929–937.
[33] S. Guda, C. Wang, M. Nehrir, Modeling of microturbine power generation systems, Electr. Power Compon. Syst. 34 (9) (2006) 1027–1041.
[34] H.R Muhammad, Power Electronics Handbook, Prentice Hall Inc, 2001, pp. 64–66.
[35] Slotine, E. Jean-Jacques, Weiping Li, Applied Nonlinear Control 199 Prentice-Hall, Englewood Cliffs, NJ, 1991 No. 1.